The final event sample is defined by the lepton selection, the vertex selection, the b-hadron selection, and the $b \to \ell$ decays selection. After all these criteria are applied, 74026 events are selected in the data. The sample composition is evaluated from simulated $Z \to q\overline{q}$ events as in Table 6.5.

$(98.6 \pm 0.4)\%$ $b\overline{b}$	$(1.15 \pm 0.03)\%$ $c\overline{c}$	$(0.25 \pm 0.02)\%$ $u\overline{u}$, $d\overline{d}$, $s\overline{s}$

Table 6.5: Final Sample composition.

The selected b-hadron hemispheres are divided in four different classes according to the process which originates the lepton candidate, as shown in Table 6.4.

The number of events selected in the data sample can be compared to the 79867 events expected from the $Z \to q\overline{q}$ simulated samples. An excess of 8% is found in the simulation. No significant difference is observed between the electron and muon selections. Some of the branching ratios for the production of b-hadrons have measured uncertainties of the order of a few percent. The corresponding systematic uncertainties are discussed in Section 8.2. The overall selection efficiency also depends on the average b-hadron lifetime, but the analysis is to first order insensitive to that. From this point onwards in this Chapter, all data/simulation comparisons are made with the number of events in the simulation normalized to that found in the data.

The vertex class population is shown in Fig. 6.25; the data distribution is compared to the expectation from the simulation. The fraction of B_s decays expected for each class is shown as well (Fig. 6.25c). A significant difference on the B_s fraction is observed between the vertex classes, in particular, the 3 classes with an odd number of charged particles in the charmed object have a B_s fraction close to 13%.

6.7 Proper time measurement

The proper time of the b-hadron at decay is computed as

$$t \;=\; l\, m_{\rm B} \,/\, p_{\rm B}\, c \;, \tag{6.4}$$

where l is the decay length estimated as explained in Section 6.3.6, $m_{\rm B}$ is the mass of the b-hadron, (taken to be $5.3\,{\rm GeV}/c^2$) and $p_{\rm B}$ is the estimate of the b-hadron momentum performed as described in the next Section.

6.7.1 Momentum measurement

The b-hadron momentum is estimated from three ingredients, *i*) the energy of the lepton candidate; *ii*) the energy of the charmed particle; and *iii*) the estimate of the neutrino energy.

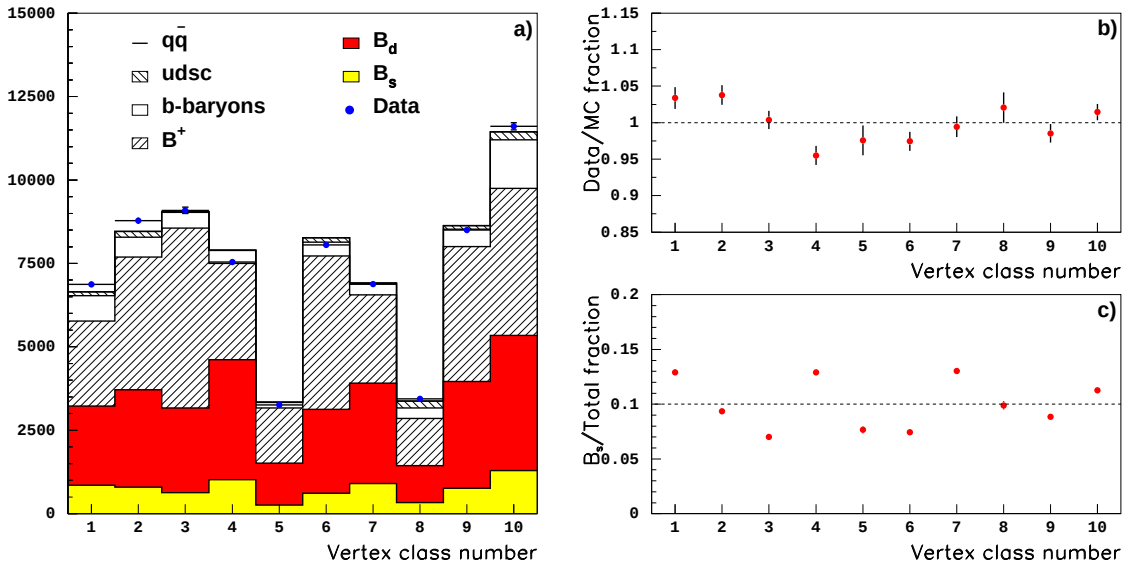

Figure 6.25: a) Distribution of the events in the selected sample in the vertex classes. The simulation histogram is normalized to the number of events selected in data.
b) Fraction of data selected events with respect to the simulation expectations for each class; some class-to-class differences are seen, but are compatible with being due to statistical fluctuations.
c) Fraction of B_s events in each class.

Charmed particle energy

The energy of the charmed particle, E_c, is estimated from a nucleated jet (Section 5.2.2) clustered around the charged particles at the charm vertex until a mass of $2.7\,\mathrm{GeV}/c^2$ is reached. Particles with momentum smaller than $0.5\,\mathrm{GeV}/c$ are excluded because they are more likely to come from fragmentation than from the b-hadron decay. This method was already used in Ref. [10].

Neutrino energy

The energy of the neutrino, E_{miss}, is estimated from the total energy and momentum conservation. If a neutrino in the lepton hemisphere is considered to be the only contribution to the unmeasured momentum in the event, the following equation holds,

$$E_{\mathrm{miss}} = \frac{\sqrt{s}}{2} + \frac{m_1^2 - m_2^2}{2\sqrt{s}} - E_1 \ . \tag{6.5}$$

The hemisphere masses m_i are determined from the measured energies E_i and momenta p_i ($m_i^2 = E_i^2 - \vec{p_i}^{\,2}$), where $i = 1$ denotes the lepton hemisphere, $i = 2$ the opposite hemisphere, and $\sqrt{s}$ is the centre-of-mass energy. This method was first used in ALEPH in Ref. [84].

The neutrino energy resolution obtained on $b \to \ell$ simulated events is shown in Fig 6.26.

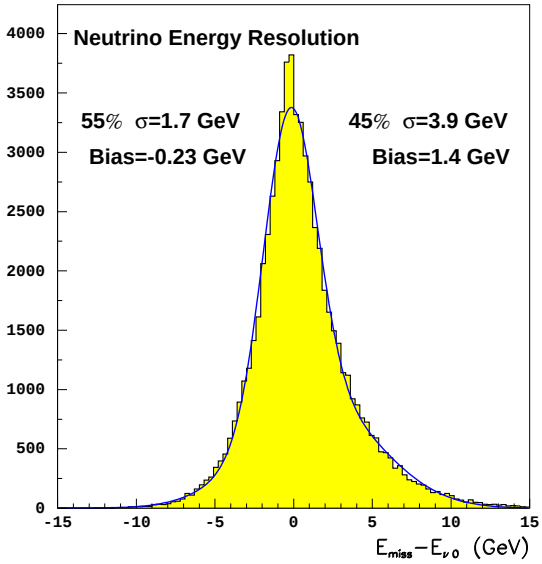

Figure 6.26: Neutrino energy bias on b $\to \ell$ simulated events. The distribution is fit with the sum of two Gaussians, their fractions and widths are indicated on the plot.

The b-hadron momentum

Once the energy of the charmed particle and the neutrino energy are determined, the b-hadron momentum is obtained as

$$p_{\mathrm{B}} \;=\; \sqrt{(E_{\mathrm{c}} + E_{\mathrm{miss}} + E_{\ell})^2 \;-\; {m_{\mathrm{B}}}^2} \;, \tag{6.6}$$

where E_ℓ is the energy of the lepton.

The b-hadron momentum obtained with this method is found to have a bias with respect to the true momentum, increasing with the measured neutrino energy. The estimate of the charmed particle energy was optimized to obtain the best b-hadron momentum resolution possible. However this optimization was performed independently of the neutrino energy, this fact explains the bias observed. A correction is applied to account for this effect. Sizeable differences on the bias are observed upon the vertex classes. A specific correction is therefore applied to each of them. The typical dependence of the momentum bias on the neutrino energy is shown in Fig. 6.27.

The improvement brought by the bias correction is shown in Fig. 6.28. The correction reduces the global bias of the distribution and also improves the resolution.

The average relative momentum resolution for all selected events in a sample of simulated $\mathrm{B_s} \to \ell$ events is shown in Fig. 6.28b: 60% of the events are found in a core with 6.4% relative momentum resolution, and 40% in a tail with 20% resolution. However, these values are not used for the oscillation fit. The momentum resolution cannot be measured event by event and a parametrization is needed. The vertex classes are also used here to divide the sample in phase space regions which contain events with similar properties. For each class, the sample is divided in bins of lepton momentum. A double Gaussian fit is performed to the relative

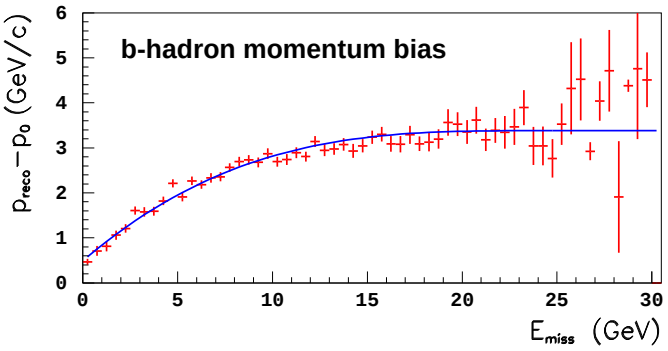

Figure 6.27: Average bias on the b-hadron momentum as a function of the neutrino energy.

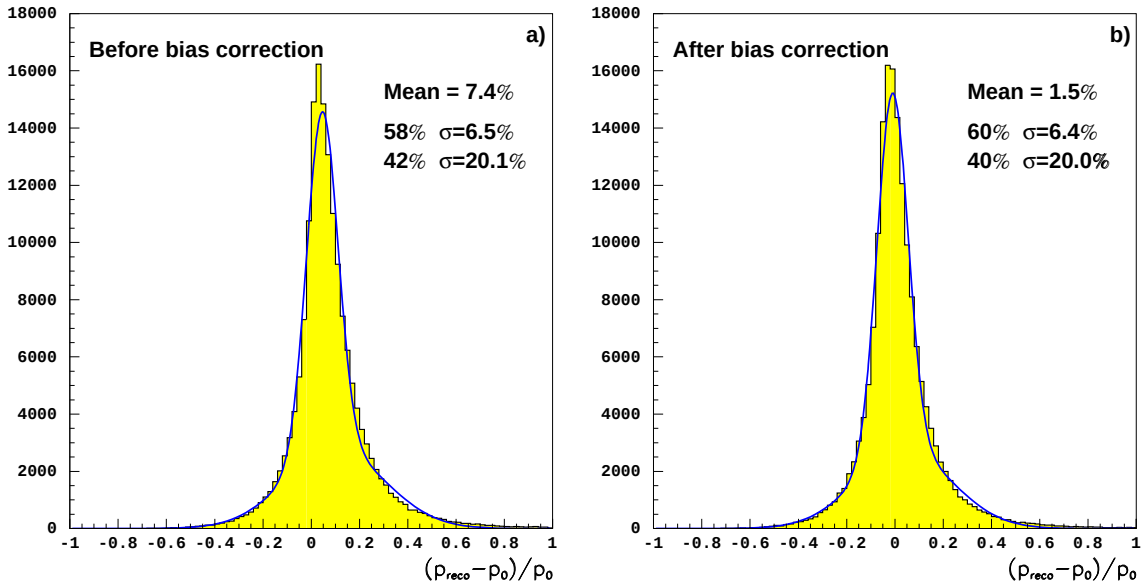

Figure 6.28: Relative momentum bias, a) before, and b) after average-bias correction. The distributions are fit with the sum of two Gaussians. Their fractions and widths are indicated on the plot along with the mean of the distributions.

momentum resolution distribution in each of these bins. The dependence of the widths of these Gaussians on the lepton momentum is parametrized with a straight line.

The relative momentum resolution distributions for two classes are given in Fig. 6.29 for illustration. Figure 6.29a contains events from a class with very good resolution (60% core at 5% and tails at 13%) and Fig. 6.29b from another class with poor resolution (53% core at 7% and tails at 22%). With the parametrization explained above, a more refined treatment of the events is achieved and the best 10% events in the first class are found to have a core resolution of 4% and tail resolution of 8% (with core and tails in the same proportion of 60% to 40%).

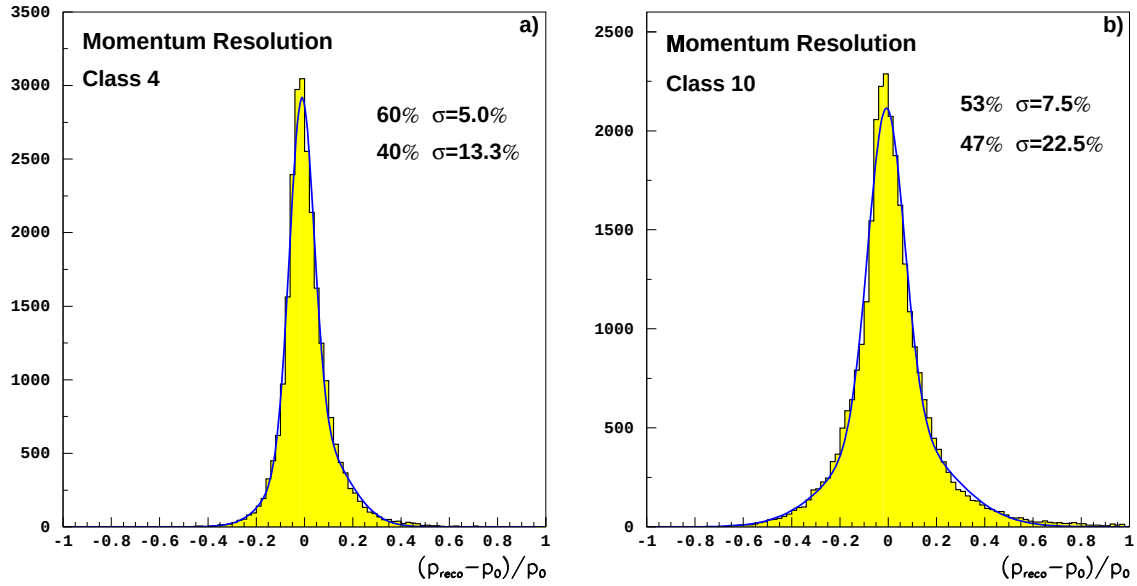

Figure 6.29: Relative momentum resolution, a) vertex class 4, and b) vertex class 10. The distributions are fit with the sum of two Gaussians. Their fractions and widths are indicated on the plot.

All corrections and parametrizations, both for the momentum measurement and for the estimation of its uncertainty, were performed on $B_s \to \ell$ simulated events.

6.7.2 Proper time

The estimate of the proper time for every selected event is obtained with Eq. 6.4 and the estimates of the reconstructed decay length and momentum. The proper time distribution for all selected events is shown in Fig 6.30, the simulation distribution is in agreement with that of the data.

The estimate of the proper time uncertainty is obtained from the convolution of the decay length uncertainty and the relative momentum uncertainty (Sections 6.3.7 and 6.7.1) as:

$$\sigma_t = \sqrt{\left(\frac{m_B}{p\,c}\,\sigma_l\right)^2 + \left(t\,\frac{\sigma_p}{p}\right)^2}\,. \tag{6.7}$$

The distribution of the estimated proper time uncertainty, σ_t, for the selected data sample is shown in Fig 6.31.

6.7.3 Proper time efficiency

The vertex selection efficiency (Section 6.3) is a function of the decay length of the b-hadron candidate. This dependence results in a non-flat proper time efficiency as a function of the

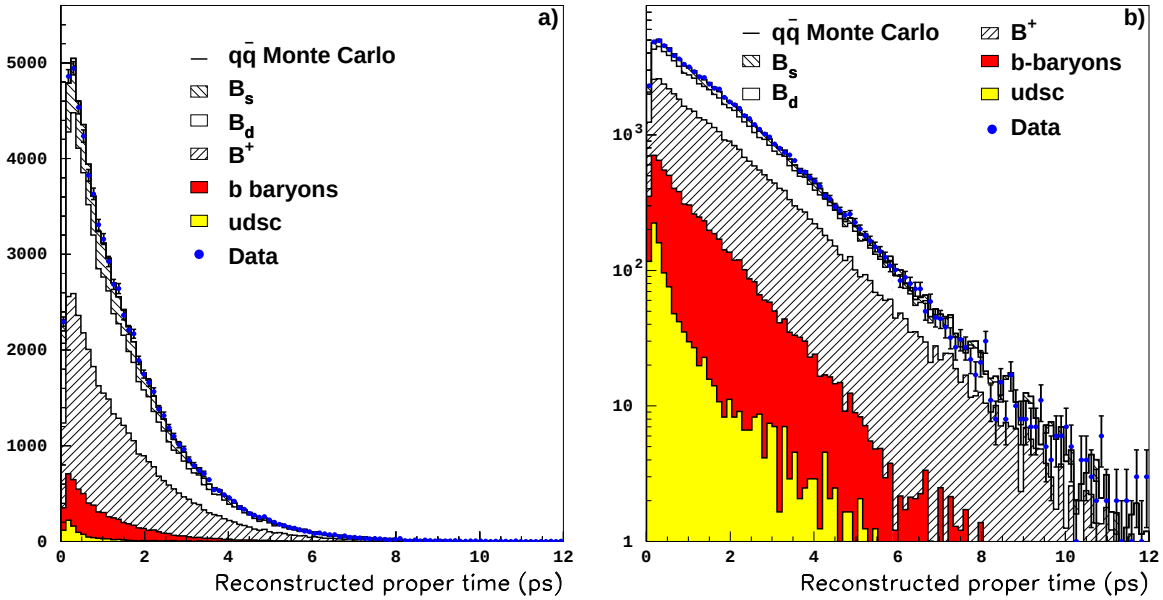

Figure 6.30: Proper time distribution in the selected sample.

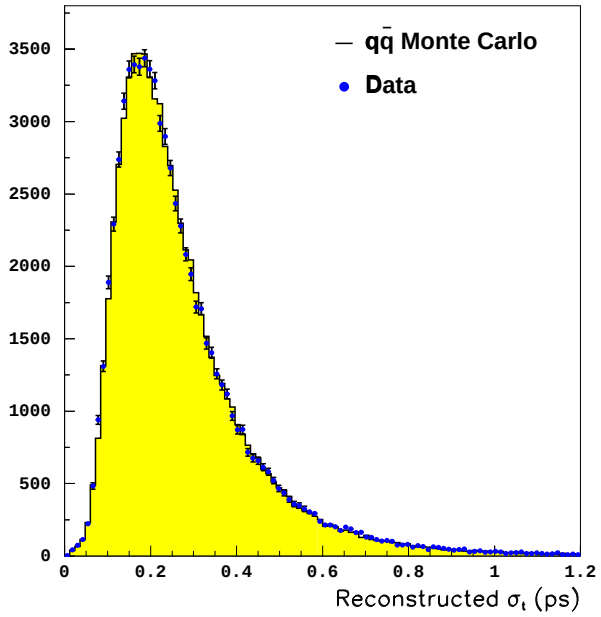

Figure 6.31: Distribution of the uncertainty on the proper time in the selected sample.

true proper time. The shape of the proper time efficiency needs to be taken into account in the oscillation fit. To this end, it has been parametrized for each vertex class and each b-hadron species.

As an illustration, the global (all vertex classes together) proper time efficiency as a function of the true proper time is shown in Fig. 6.32 for $B_s \to \ell$ signal Monte Carlo events.

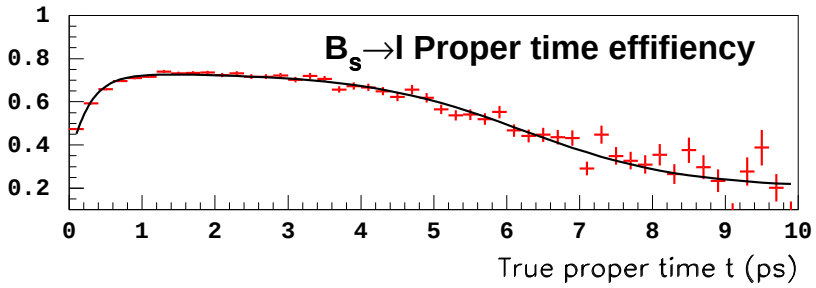

Figure 6.32: Proper time efficiency for $B_s \to \ell$ simulated events, with the parametrization superimposed.

6.8 Kaon identification

The presence of kaon candidates is used in this analysis for the B_s enrichment (Section 6.9) and for the initial state tag (Section 6.10). Charged and neutral kaons are used in the first case, and only charged kaons in the second. In this Section, the procedure used for kaon identification is explained. A jet clusterization with the JADE algorithm and $y_{\rm cut} = 0.02$ is performed to obtain jets which contain all the b-hadron decay products and the fragmentation particles closest in phase space with the b-hadron. In the B_s decay hemisphere, all kaons are searched for inside the jet which contains the lepton and the charmed particle. This jet is called "big" jet in what follows.

6.8.1 Charged kaons

Charged kaons are searched for in the two event hemispheres. In the B_s candidate hemisphere, kaons issued from both the B_s fragmentation process and from its decay can be exploited for flavour tagging and/or B_s enrichment. In the opposite hemisphere, only decay kaons are relevant for flavour tagging.

Charged kaons are distinguished from other charged particles by their dE/dx measurement in the TPC. The separation between fragmentation and decay kaons is done with the same variables used for the general track separation (Section 6.3.2). However, for those events where a charm vertex is reconstructed, the impact parameter significance with respect to this vertex (rather than the tertiary vertex seed) along the charmed particle flight direction is taken as a variable to measure its compatibility with originating from the b-hadron decay.

A neural network is used to combine the dE/dx estimator with the track separation variables. A different treatment is introduced for charged particles included in the charm track selection and for the others. In the first sample, only decay kaons are expected, because the contamination from fragmentation particles can be neglected. A special network is trained on this track sample. In the case of tracks not included in the charm selection, the network is trained to distinguish three track classes: charged kaons from fragmentation, charged kaons from the B_s decay, and non-kaon particles. Both neural network trainings are performed using tracks included in the "big" jet of $B_s \to \ell$ selected simulated events. The combined estimator distributions for fragmentation kaons, and for decay kaons in the charm track selection are shown in Fig 6.33.

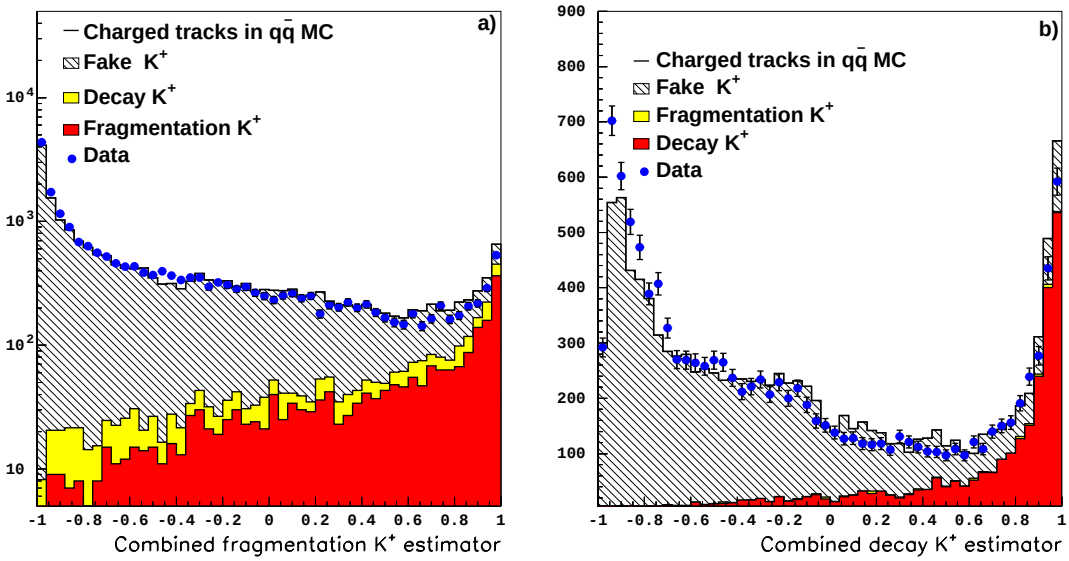

Figure 6.33: Charged kaon estimators, a) for a fragmentation kaon, and b) for a kaon from the b-hadron decay in the charm track selection.

The two estimators for the decay kaon are parametrized to obtain a probability for each track to be a kaon from the c-hadron decay. This probability is the estimator used in the B_s enrichment (Section 6.9).

For the opposite side hemisphere, a new estimator is built to identify kaons from the decay of any b-hadron. The same set of discriminant variables is used, and the training is done on unbiased b hemispheres.

6.8.2 Neutral kaons

Neutral kaons, K_S, both issued from the b quark fragmentation process and from the meson decay, are searched for in the B_s candidate hemisphere. Only the reconstruction of K_S into two charged pions is attempted.

In the event reconstruction, long-lived neutral particle candidates (V_0) are identified as two oppositely charged particles, each of them incompatible with originating from the primary

vertex, but compatible with being the decay products of a known neutral long-lived particle originating from the primary vertex [66]. In each event, K_S candidates are looked for in the V_0 selection. Several variables distinguish a true from a fake K_S, their list follows. *i*) The mass of the reconstructed neutral particle; *ii*) its distance of flight from the primary vertex; *iii*) the χ^2 of the fit of each pion with the primary vertex; *iv*) the χ^2 of the K_S mass constrained fit; *v*) the reconstructed K_S momentum; *vi*) the distance of closest approach between the helices of the two charged pions; and *vii*) the angle between the reconstructed K_S momentum and its flight direction. The distributions of all these variables, for V_0 candidates in data and simulation are shown in Figs. 6.34 to 6.37.

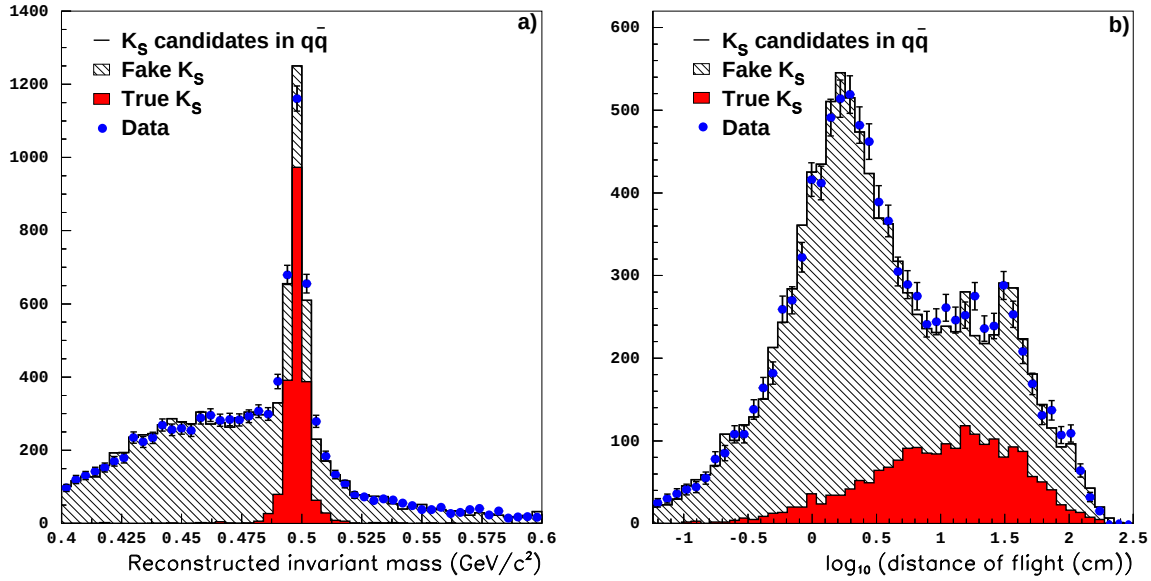

Figure 6.34: K_S estimators a) K_S reconstructed mass, and b) K_S distance of flight (the logarithm of the distance is plotted).

Only K_S candidates with a reconstructed mass within $30\,\mathrm{MeV}/c^2$ from the nominal value ($m_{K_S} = 497.672 \pm 0.031\,\mathrm{MeV}/c^2$ [13]) are considered. The discriminant variables listed above are combined with kinematical variables (estimators of the angle with the b-jet, and compatibility with the primary and tertiary vertices, as for the track separation described in Section 6.3.2) to obtain an estimator for both fragmentation and decay neutral kaons. The combination is performed with a neural network, the training of which is performed on K_S candidates in $B_s \to \ell$ selected simulation events. The combined neutral kaon estimator distributions for kaons issued from the b fragmentation process and from the b-hadron decay are displayed in Fig. 6.38.

With a cut at zero on each estimator, 90% of the pion pairs selected are found to originate from K_S's. Out of those, 70% originate from the b-hadron decay in the case of the decay K_S estimator, and 90% come from the b quark fragmentation in the case of the fragmentation K_S estimator.

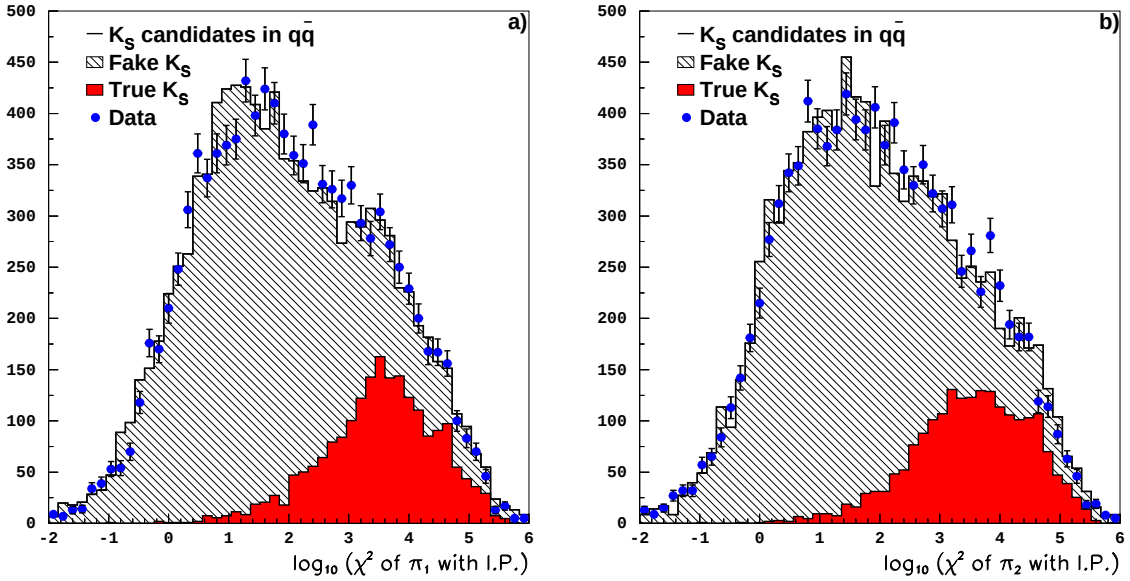

Figure 6.35: The χ^2 of the two decay pions with the primary vertex (the logarithm of the χ^2 is plotted).

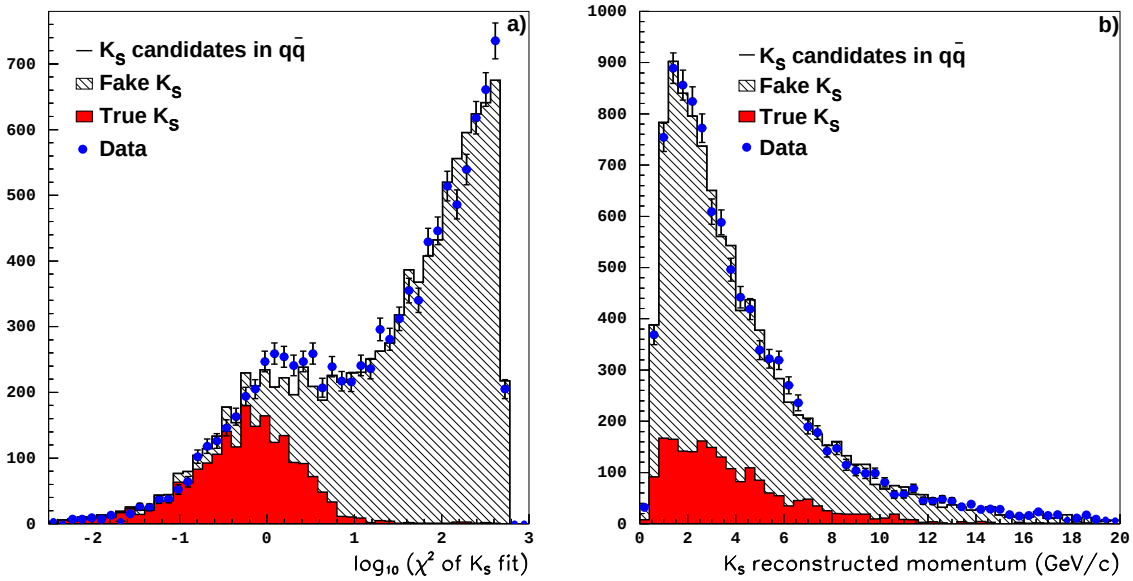

Figure 6.36: K_S estimators a) χ^2 of the K_S mass constraint fit (the logarithm is plotted), and b) K_S reconstructed momentum.

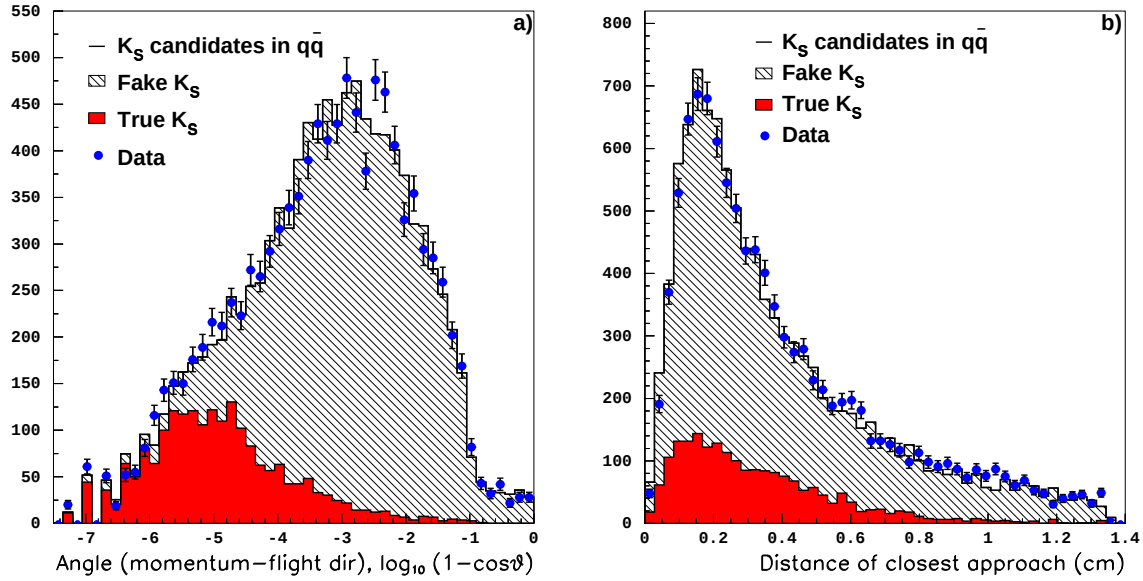

Figure 6.37: K_S estimators a) angle between the momentum and the flight direction of the K_S candidate, and b) distance of closest approach between the two pion helices.

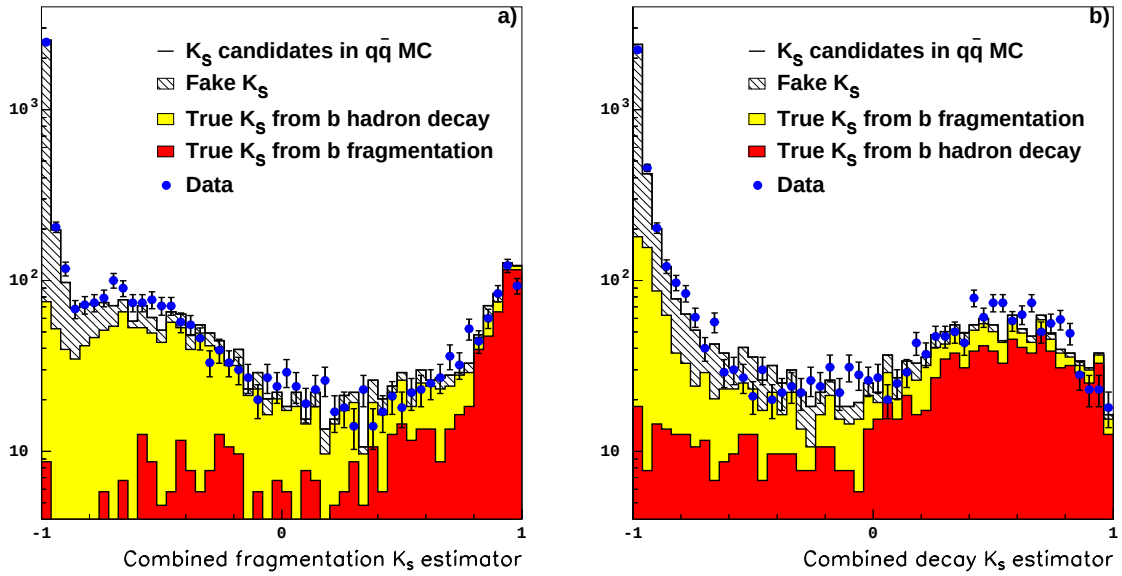

Figure 6.38: Combined neutral kaon estimators, a) for K_S from fragmentation, and b) for K_S from the b-hadron decay.

6.9 B_s enrichment

In an unbiased b-hadron sample only about 10% of the hemispheres contain a B_s [13]. The sensitivity of the oscillation analysis can be improved through the identification of variables which discriminate B_s from other b-hadron decays, and the evaluation, event by event, of the probabilities that a given candidate belongs to each b-hadron species.

The B_s enrichment proceeds in two streams: *i*) variables related to the electric charge and the charge particle multiplicity of the secondary and tertiary vertices distinguish charged from neutral b-hadrons; *ii*) the presence of kaons among fragmentation and decay particles distinguish B_s decays from the other b-hadrons. For the charged decay kaons, the charge correlation with the lepton candidate is the best discriminant.

A set of discriminant variables is identified and combined with a neural network to obtain an optimal separation performance. The description of the variables in the two streams follows.

Separation between charged and neutral b-hadrons

The number of charged particles in the charm vertex distinguishes between neutral and charged b-hadrons. With the assumption of perfect charged particle separation between those originated from the b-hadron decay and the others, an odd number of charged particles is expected in the charm vertex for neutral b-hadrons, and an even number for charged b-hadrons.

A new charged particle separation variable is built, based on the same particle properties as that described in Section 6.3.2. Two modifications are introduced to improve its performance. On one hand, the neural network training is done exclusively on events which fulfil all the selection criteria described in the previous Sections, and on the other, the impact parameter significance with respect to the charm vertex (if any) is taken as a variable to measure the compatibility of a charged particle with originating from the b-hadron decay. If no charm vertex is reconstructed, the impact parameter significance with respect to the inclusive tertiary vertex is used, as in Section 6.3.2. This track separation variable is used to build a set of "weighted" charm vertex estimators: the secondary vertex charge, the weighted vertex multiplicity, and the charge weighted momentum. The definition of these three estimators follows.

$$\text{Vertex charge} = q_\ell \sum_i^{N_{\rm ch}} w_i^{\kappa_1}\, q_i \ , \tag{6.8}$$

$$\text{Vertex multiplicity} = \sum_i^{N_{\rm ch}} w_i^{\kappa_2} \ , \tag{6.9}$$

$$\text{Charge weighted momentum} = q_\ell \sum_i^{N_{\rm ch}} w_i\, p_i^{\kappa_3}\, q_i \ , \tag{6.10}$$

In the three expressions, $N_{\rm ch}$ is the number of charged particles in the hemisphere, w_i is the value of the track separation variable for the i-th particle (expected to be close to 1 for true decay particles and close to 0 otherwise), p_i is the momentum of the i-th particle, q_i is the

charge of the i-th particle, q_ℓ is the charge of the lepton, and the κ_j values are optimized to obtain the best separation performance, ($\kappa_1 = 1.6,\ \kappa_2 = 2.2,\ \kappa_3 = 1.1$). The vertex charge is expected to be peaked at -1 for neutral b-hadrons (the charmed particle and the lepton have opposite electric charge sign) and at zero otherwise. The vertex multiplicity is expected to be concentrated around integer odd values for neutral b-hadrons. The charge weighted momentum distribution is expected to have a negative mean for neutral b-hadrons, and to be centred at zero otherwise.

The distributions of these variables in data and simulation are shown in Figs. 6.39 and 6.40. The fraction of B_s events in the simulation as a function of each variable is also displayed.

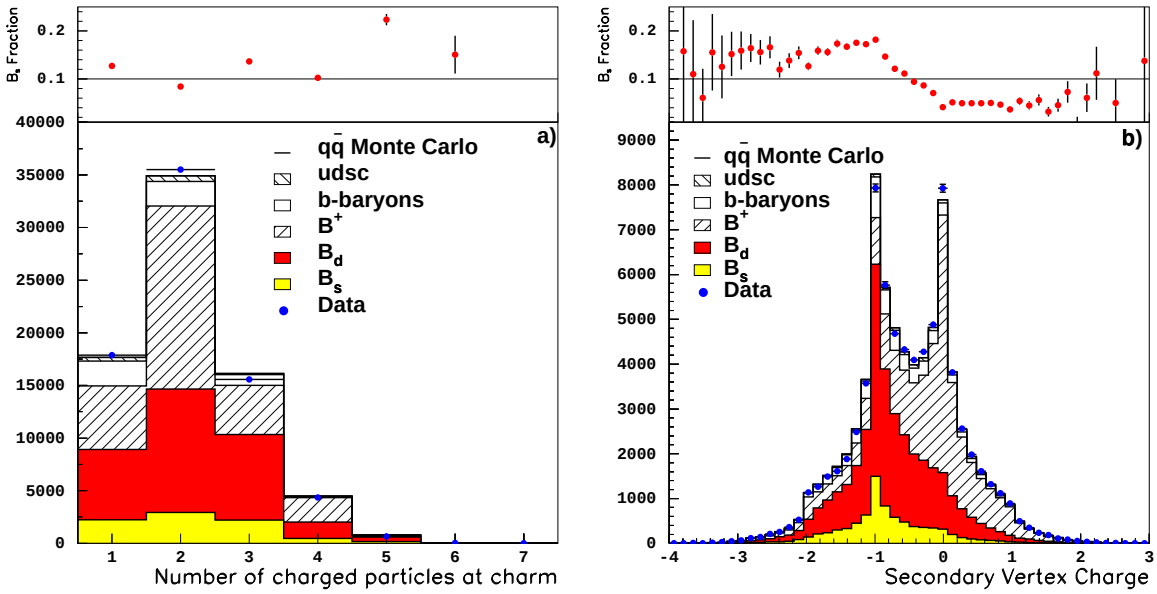

Figure 6.39: a) Number of charged particles at the charm vertex, and b) charm vertex charge estimator.

Separation between B_s and other neutral b-hadrons

The presence of a kaon among the fragmentation particles is an indication of a B_s decay. The fragmentation kaon can be charged or neutral. A variable is defined to identify charged kaons and another for K_S issued from the fragmentation process. For the charged fragmentation kaon, all tracks inside the "big" b-jet (Section 6.8) and not included in the charmed track selection are considered. The track with the highest value of the fragmentation kaon estimator (Section 6.8.1) is chosen and its estimator value is taken as a discriminant variable for the B_s enrichment. A similar treatment is applied to identify neutral kaons. The distributions of the fragmentation kaon estimators in data and simulation, and the fraction of B_s events as a function of the these estimators, are shown in Fig. 6.41.

The decay products of a semileptonic B_s decay include, in most cases, two kaons from the D_s^- decay, while the B_d decay products include typically a single kaon at most (apart from

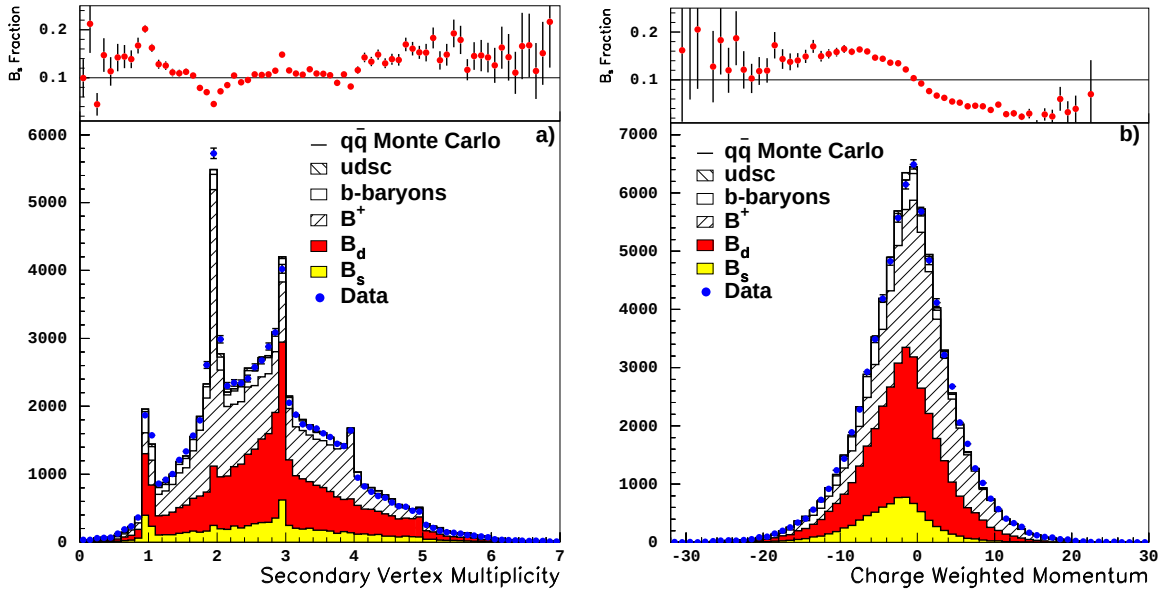

Figure 6.40: a) Charm vertex weighted multiplicity, and b) charm vertex charge weighted momentum estimators.

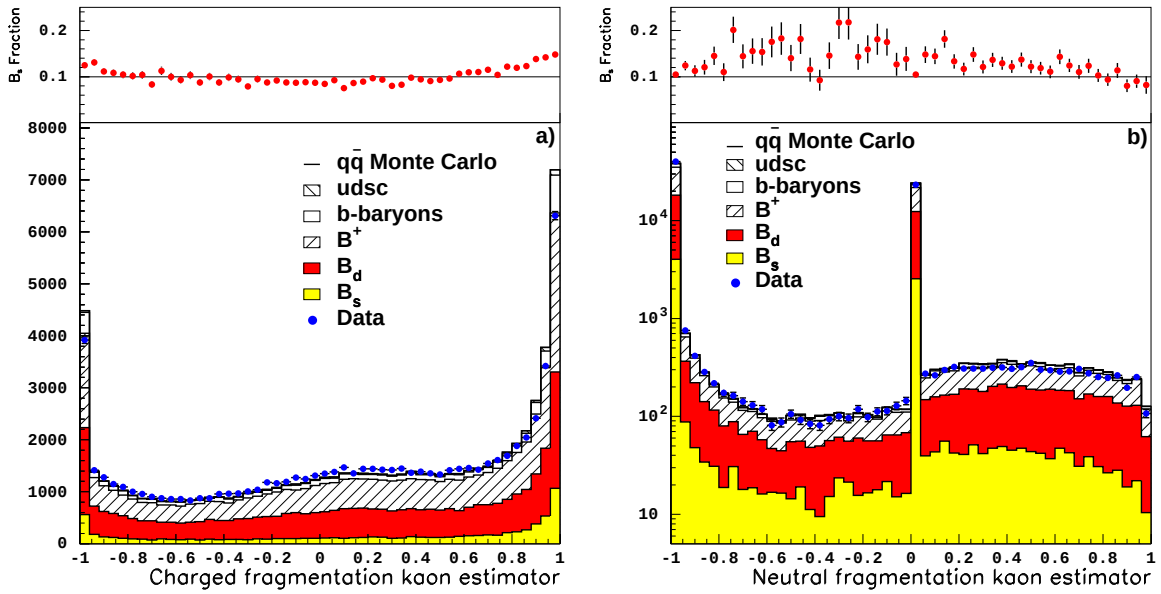

Figure 6.41: Fragmentation kaon estimators, a) charged kaon candidate, and b) neutral kaon candidate.

rare decays, thus not relevant here). The number of kaons found in the decay products of the b-hadron therefore distinguishes B_s decays from other b-hadron decays. Moreover, charged kaons from B_d decays have the same electric charge sign as the lepton, while in the case of B_s decays approximately the same amount of charged kaons of each sign are expected. The presence of a ϕ among the b-hadron decay products is a clear tag for a B_s decay. Finally, these properties are addressed by the variables defined below.

- Largest charged kaon candidate estimator for kaons with electric charge sign opposite to that of the lepton.
- Largest charged kaon candidate estimator for kaons with the same electric charge as the lepton.
- Largest two neutral kaon estimators.
- Invariant mass of the best (according to the kaon estimator) oppositely charged kaon pair formed to look for a ϕ candidate.
- $\sigma = \sum_i w_i\,(1 - w_i)$ the track separation estimator for the hemisphere, used as control variable.

The distributions of all these variables in data and simulation, and the fraction of B_s events as a function of the discriminant variables are shown in Figs. 6.42 to 6.44.

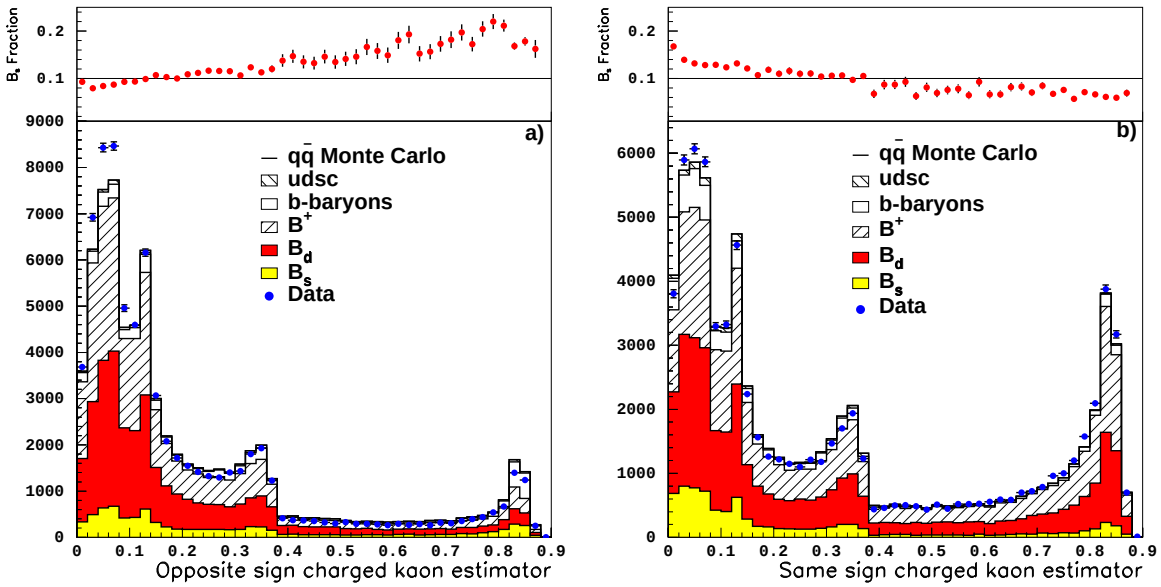

Figure 6.42: Charged decay kaon estimators, a) kaon with charge opposite to that of the lepton, and b) kaon with the same charge as the lepton.

The above twelve variables are combined with a neural network. The training is performed with $B_s \to \ell$ events as signal, and $b \to \ell$ decays, where the b quark forms any other b-hadron, as background. The distribution of the combined variable, N_{enrich} in data and simulation is shown in Fig. 6.45.

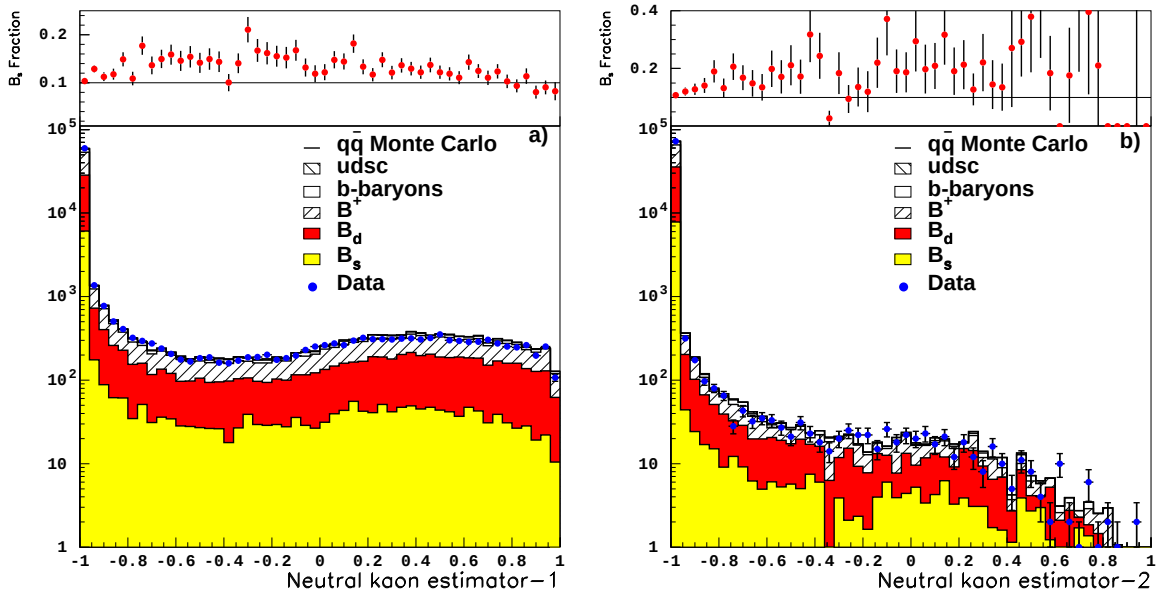

Figure 6.43: Neutral decay kaon estimators for, a) the best candidate, and b) the second best candidate (if any). The variable is set to zero when no neutral candidate is found.

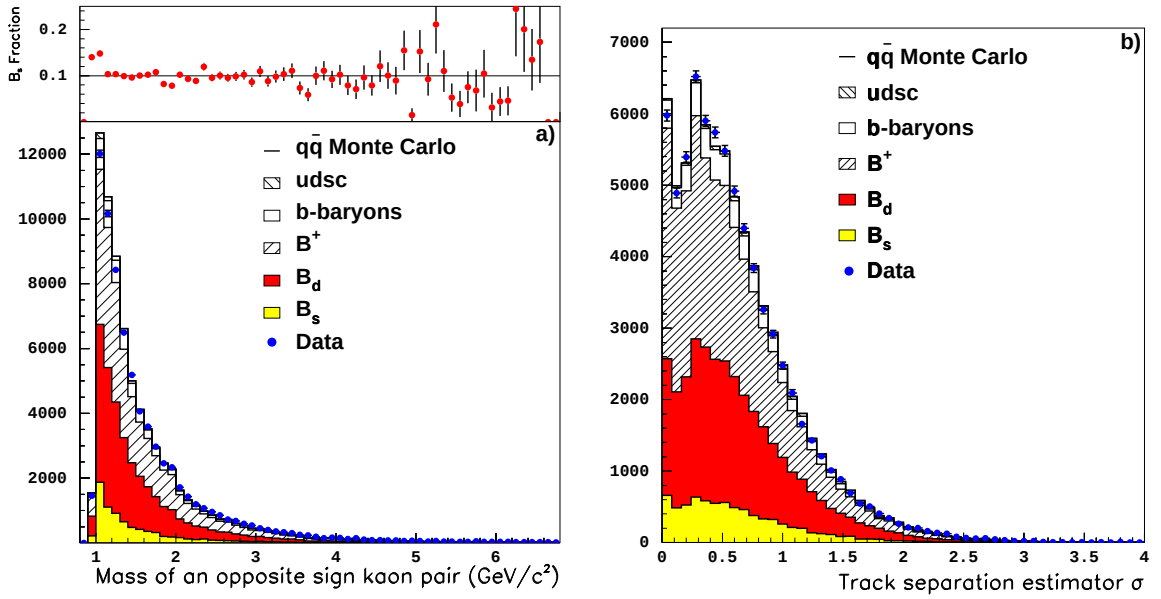

Figure 6.44: a) Invariant mass of the best ϕ candidate, and b) charged particle separation estimator in the B_s hemisphere.

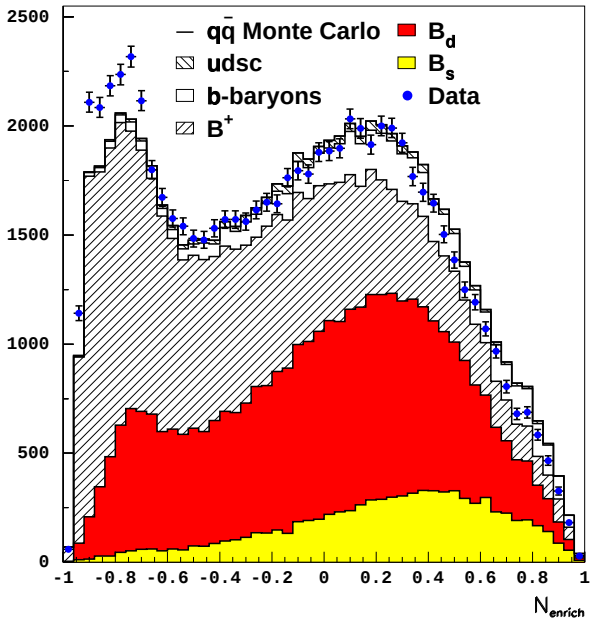

Figure 6.45: Combined enrichment variable.

A disagreement between data and simulation is seen the N_{enrich} distribution. A deficit of simulated events in the region mostly populated by B^+ mesons is observed. Although the biggest discrepancy between data and simulation in the input variables is seen in the charged decay kaon estimators (Fig. 6.42), a problem with the kaon identification is not expected to differentiate between charged and neutral b-hadrons. The explanation must therefore involve the charge estimators. All input charge estimators (Figs. 6.39 and 6.40) used to separate neutral from charged b-hadrons show some disagreement between data and simulation. In all cases, this disagreement favours the hypothesis of having less charged b-hadrons selected in the simulation than in the data.

The secondary vertex charge variable (Fig. 6.39b) was used to fit the amount of charged and neutral b-hadrons seen in the data sample selected. This distribution obtained from the simulation was found to fit nicely the data if the fraction of charged b-hadron was increased by 8%. All the variables which distinguish charged from neutral b-hadrons show a better agreement data/simulation with this adjustment. The distributions of the charge estimators with the correction applied are shown in Figs. 6.46 and 6.47.

The distribution of N_{enrich} after this correction (Fig. 6.48) still shows some deviation, which is however reduced by more than a factor of two with respect to the original one. This residual discrepancy is probably due to differences in shape for the variables that distinguish B_s decays from the other neutral b-hadrons (in particular for the charged kaons estimators). The effect of a difference in shape on the event-by-event estimated B_s purity is smaller than the effect of a bias in the selection efficiency. A possible systematic effect due to the residual discrepancy is estimated by removing the weights which re-adjust the charged-to-neutral ratio (Section 8.2).

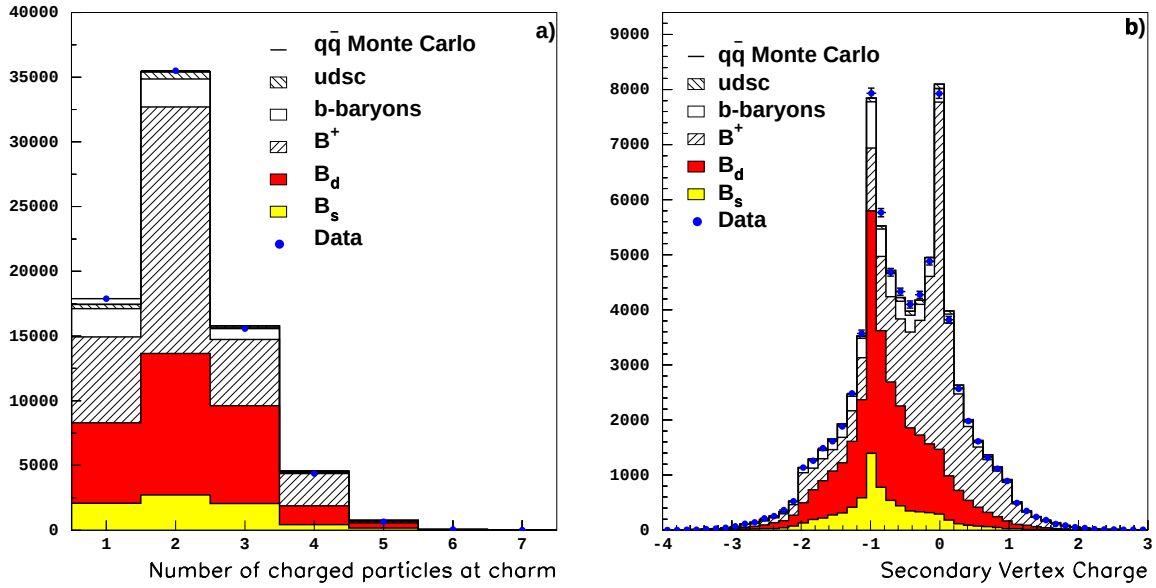

Figure 6.46: a) Number of charged particles at the charm vertex and b) charm vertex charge. Simulated events are reweighted to increase by 8% the B^+ population, as favoured by the data.

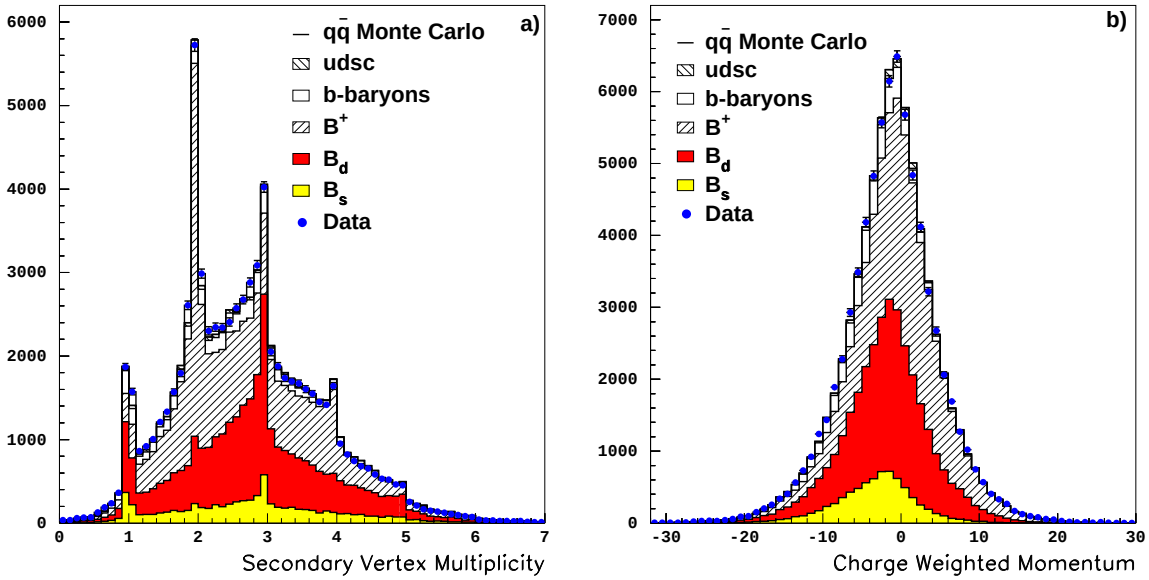

Figure 6.47: a) Charm vertex weighted multiplicity, and b) charm vertex charge weighted momentum. Simulated events are reweighted to increase by 8% the B^+ population, as favoured by the data.

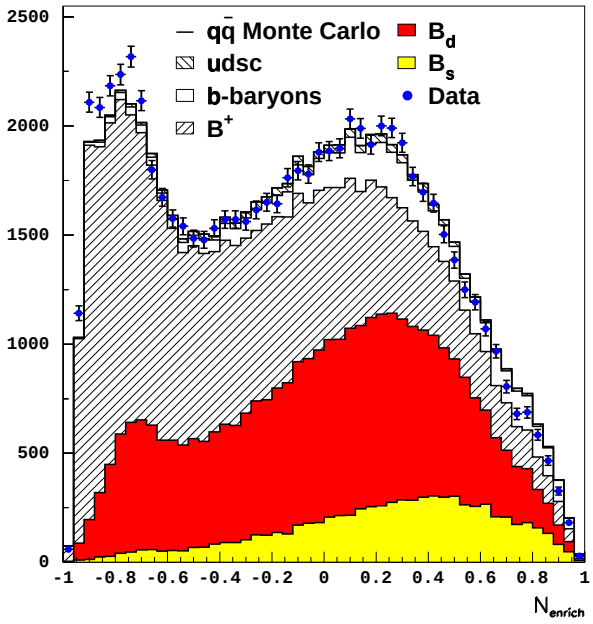

Figure 6.48: Combined enrichment variable with simulated events reweighted to increase by 8% the B^+ population, as favoured by the data.

The B_s enrichment estimator is used event by event to get the probability for the candidate to be a B_s, B_d, B^+, or b-baryon decay. In Fig. 6.49 the probability of each b-hadron species is shown as a function of the enrichment estimator. For approximately half of the event sample ($N_{\text{enrich}} > 0$) the B_s purity is estimated to be higher than the average 10%. For 17% of the events ($N_{\text{enrich}} > 0.4$), it is 20% or higher. The effective increase of the B_s purity on the whole sample is evaluated to be $\sim 25\%$.

6.10 Initial state tag

The B_s oscillation analysis requires the determination of whether the selected b-hadron contains a b or a $\bar{b}$ quark at production time. This determination is achieved with a study of the properties of the whole event, with the exclusion of the lepton candidate and the other b-hadron decay particles.

Properties of the hemisphere opposite to the semileptonic decay are used to determine the $b/\bar{b}$ content of the b-hadron produced together with the B_s candidate, and thus to indirectly determine the production state of the B_s candidate. The same side hemisphere carries information on the fragmentation process which produces the B_s candidate, and can also be used in the initial state flavour determination.

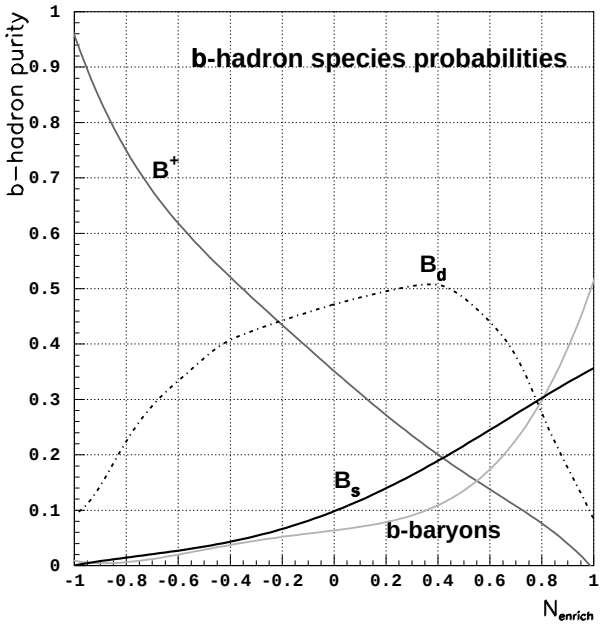

Figure 6.49: Probability of each b-hadron species is shown as a function of N_{enrich}.

6.10.1 Opposite hemisphere

The hemispheres opposite to the $B_s \to \ell$ candidate are unbiased b-hadron decays. Therefore a "general purpose" method for flavour tagging has to be used. The method described here was developed to study B_s oscillations and CP violation in the B_d system [85].

The calculation of the flavour estimator starts with the jet reconstruction. The JADE algorithm is used with a jet-resolution parameter $y_{\text{cut}} = 0.02$. The jet which includes the selected $B_s \to \ell$ candidate is identified and the jet which forms the highest invariant mass with this B_s jet is selected in the opposite hemisphere. The b-hadron decay vertex is searched for with a topological vertexing algorithm (either VNFIT or QVSRCH). This vertex is constrained to be on the axis of the selected jet in the hemisphere. Each track is then assigned a relative probability $\mathcal{P}_v$ that it originates from the secondary vertex.

The JADE jet definition with $y_{\text{cut}} = 0.0044$ is used to estimate the b-hadron flight direction. If more than one jet is found in the hemisphere considered (opposite to the B_s candidate), the b-jet candidate is chosen on the basis of the kinematic properties of its tracks and/or the presence of lepton candidates. The leading track of the b-jet candidate is used as a seed for BTCONE. The resulting jet axis is taken as an estimate of the b-hadron flight direction. In two-jet events (with Section 6.2 definition), the thrust axis is chosen instead. The uncertainties on the reconstructed angles are parametrized as a function of the jet momentum. A second estimate of the direction is taken as the vector joining the primary and secondary vertices, and its uncertainty is parametrized as a function of the measured decay length. The two estimates are averaged using their parametrized uncertainties, and the result is taken as the final b-hadron flight direction.

The b-hadron flight direction described above is used to build a track separation estimator

similar to that described in Section 6.3.2, but optimized on unbiased b-hadron decays. The estimator is converted to a probability $\mathcal{P}_{\rm sec}$ that a track originates from the secondary vertex.

The opposite side tag is built to have similar performance for all b-hadron decays. However, the charged particle distribution in an b-hadron decay hemisphere depends on the b-hadron type (B^+, B^0, or b-baryon). A variety of charge estimators tailored to the different b-hadron decays present in unbiased hemispheres are combined with information intended to differentiate between charged and neutral b-hadron decays.

A set of nine variables sensitive to the b-hadron charge are used for the opposite side tag. Two jet charge estimators are defined using all tracks in the hemisphere.

$$Q_{\rm J} = \frac{\sum_i q_i(\vec{p}_i \cdot \vec{d}_{\rm J})^\kappa}{\sum_i (\vec{p}_i \cdot \vec{d}_{\rm J})^\kappa} , \qquad \kappa = 0.5,\, 1. , \tag{6.11}$$

where q_i and $\vec{p}_i$ are the charge and momentum of the i-th track, and $\vec{d}_{\rm J}$ is the b-hadron flight direction. The jet charge is expected to have a negative (positive) mean for generic b ($\bar{\rm b}$) -hadrons. Two secondary vertex charges, one weighted with each track momentum along the b-hadron flight direction, are defined on the whole hemisphere

$$Q_{\rm vtx} = \sum_i \mathcal{P}_{\rm sec} q_i , \tag{6.12}$$

$$Q_{\rm vtx'} = \frac{\sum_i \mathcal{P}^i_{\rm sec} q_i(\vec{p}_i \cdot \vec{d}_{\rm J})^\kappa}{\sum_i \mathcal{P}^i_{\rm sec}(\vec{p}_i \cdot \vec{d}_{\rm J})^\kappa} , \qquad \kappa = 0.3 . \tag{6.13}$$

The weighted secondary vertex charge is expected to have the same correlation with the b-hadron flavour as the jet charge. The pure secondary vertex charge distinguishes between neutral and charged b-hadrons. For charged b-hadrons, it is also sensitive to the b ($\bar{\rm b}$) content. The weighted primary vertex charge, defined as

$$Q_{\rm pri} = \frac{\sum_i (1-\mathcal{P}^i_{\rm sec}) q_i(\vec{p}_i \cdot \vec{d}_{\rm J})^\kappa}{\sum_i (1-\mathcal{P}^i_{\rm sec})(\vec{p}_i \cdot \vec{d}_{\rm J})^\kappa} , \qquad \kappa = 1.0 , \tag{6.14}$$

which also includes all tracks in the hemisphere. For charged b-hadrons, the primary vertex charge has the opposite charge correlation with the b quark, than that of the secondary vertex charge. For neutral b-hadrons, the primary vertex charge is especially important, as the secondary vertex charge provides almost no information.

Apart from the hemisphere-based charge estimators defined above, the total charge of the jet is also used. It is defined as $Q_{\rm tot} = \sum_i q_i$, where i runs over the charged particles in the b-jet. It is expected to have the same charge correlation with the b-hadron charge as the jet charge estimators.

The b ($\bar{\rm b}$) content of the b-hadron can also be estimated with $p_\parallel \cdot q$, where $p_\parallel$ is the longitudinal momentum with respect to the b-hadron flight direction of the leading particle in the b-hadron hemisphere, and q the sign of its electric charge. Identified leptons (Section 5.3) and kaons (Section 6.8.1) are also used, if present.

The variables described above are combined, together with a set of control variables ($\cos\theta_{\rm thurst}$, the charged particle multiplicity, the combined track separator estimator for the hemisphere, the reconstructed b-hadron momentum, the reconstructed decay length, and the

lepton momentum, in the case a lepton was found) with a neural network to obtain the combined opposite side tag variable. The distribution of this variable for the selected data and simulation samples are shown in Fig. 6.50.

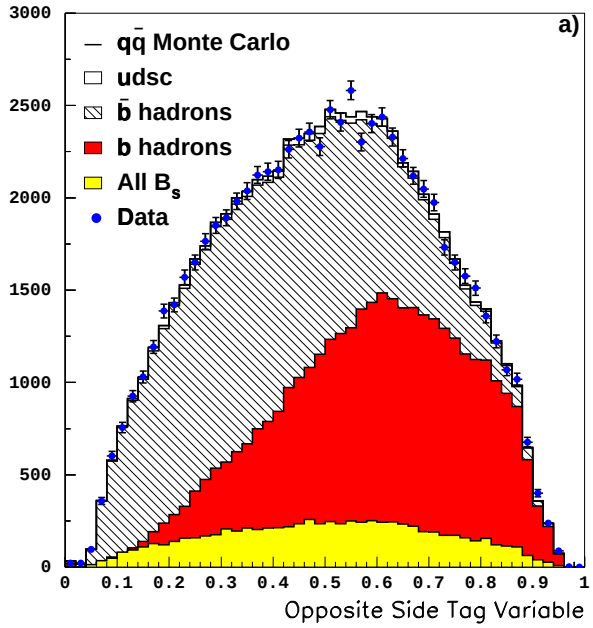

Figure 6.50: Opposite side initial state tag variable.

The effective mistag probability (defined in the next Section) for the opposite tag estimator in generic hemispheres is $\eta_{\text{eff}} = 29\%$.

6.10.2 Same hemisphere

On the B_s candidate hemisphere, flavour estimators are built as insensitive as possible to the decay products. The estimators can be divided in two types, *i*) primary vertex charge estimators, and *ii*) a charged fragmentation kaon estimator. In the first case, the estimators are built to be sensitive to the overall charge of fragmentation particles in the hemisphere of the B_s candidate. If the fragmentation kaon produced together with the B_s candidate is electrically charged, the charge sign is correlated with the b flavour of the B_s at production.

Five different estimators of the primary vertex charge are defined. Three of them use all tracks in the "big" b-jet weighted with their probability to be b-hadron decay products (defined as explained in Sections 6.3.2 and 6.9). The other two use tracks inside the same b-jet after the exclusion of the selected c tracks. These estimators are defined as

$$\begin{aligned} \text{PV Charge}_{\text{all}} &= \textstyle\sum_i^{N_{\text{jet}}} (1-w_i)\, q_i\, p_{i_\parallel}^{\kappa} \qquad \kappa = 0,\ 0.6,\ 1\ , \\ \text{PV Charge}_{\text{c excl}} &= \textstyle\sum_i^{N_{\text{jet}}} q_i\, p_{i_\parallel}^{\kappa} \qquad \kappa = 0,\ 0.3\ , \end{aligned} \tag{6.15}$$

where N_{jet} is the number of charged particles in the "big" b-jet, q_i is the charge of the i-th particle, $p_{i_\parallel}$ is the i-th particle momentum projected on the reconstructed b-hadron

flight direction. The κ values have been optimized to obtain the best overall separation performance.

The distributions of these five estimators are shown in Figs. 6.51 to 6.55. On the left (a) plots, the variable distribution is shown for all selected events, the data distribution is compared to that of simulated events; on the right (b), the variable distribution for $B_s \to \ell$ and $\overline{B}_s \to \ell$ simulated events are shown.

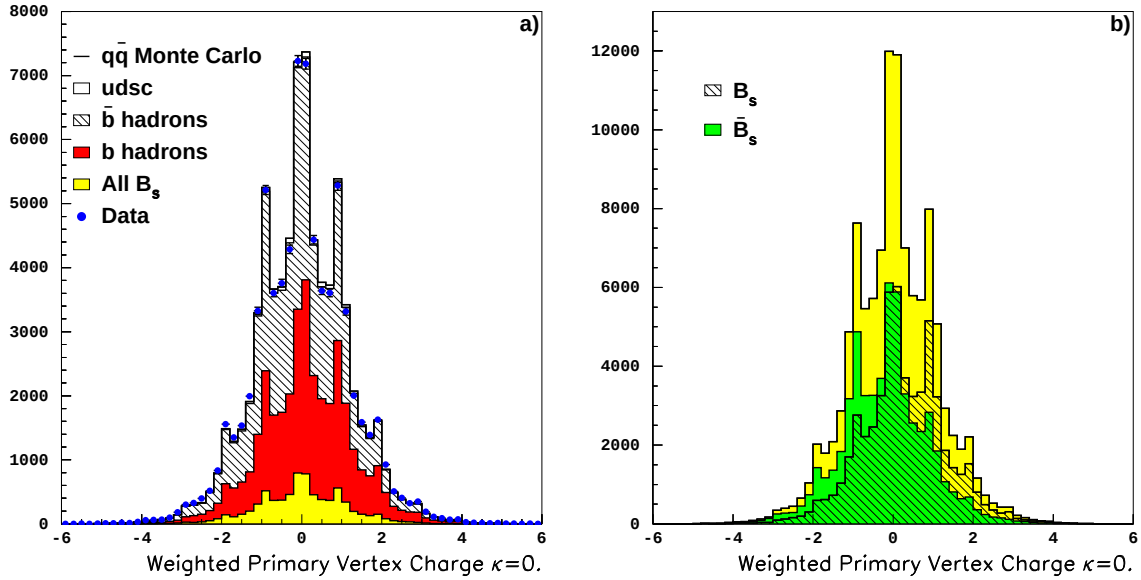

Figure 6.51: Weighted primary vertex charge with $\kappa = 0$. a) For all selected events in data and simulation, and b) for $B_s \to \ell$ simulated events.

Charged fragmentation kaons are looked for in the selected events within particles in the "big" jet but not included in the c track selection. If their fragmentation kaon estimator (Section 6.8.1) value is positive, this value multiplied by the electric charge of the kaon candidate track is taken as fragmentation kaon variable for the flavour tagging. The variable is set to zero otherwise. The distribution of the charged fragmentation estimator used here is shown in Fig. 6.56a for the selected data sample, and in Fig. 6.56b for $B_s \to \ell$ and $\overline{B}_s \to \ell$ simulated events.

In addition, some control variables are used, *i*) the measured decay length l; *ii*) the measured momentum p_B; and *iii*) $\sigma = \sum_i w_i(1-w_i)$ which estimates the quality of the track separation.

An additional variable, not specific to any of the two hemispheres, is considered. The polar angle of the event thrust axis is used as a global flavour estimator profiting from the b forward-backward asymmetry. The distribution of the signed thrust polar angle is shown in Fig. 6.57.

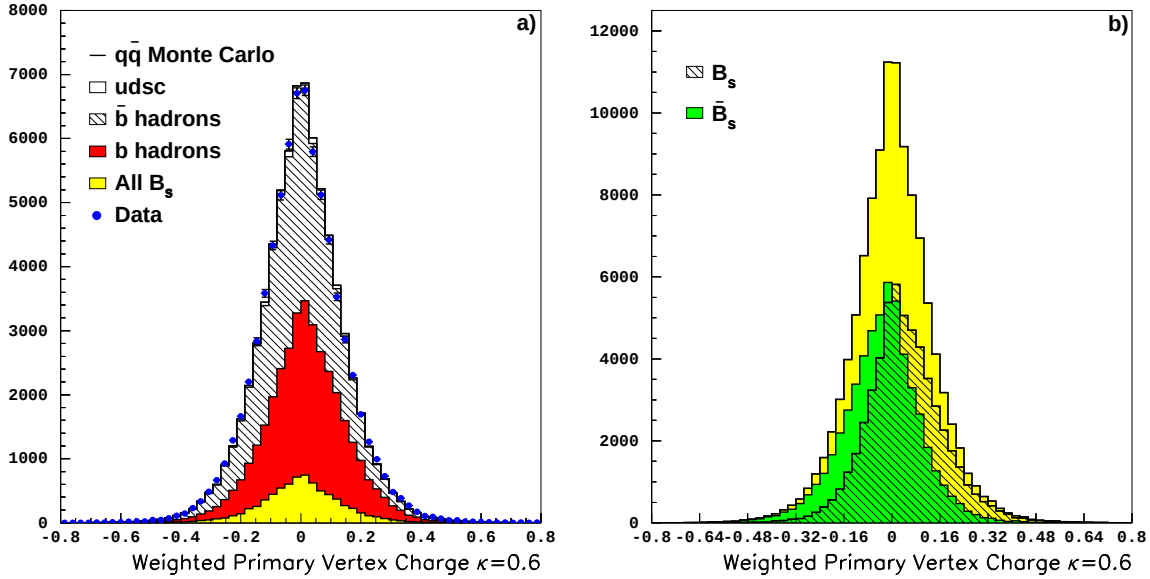

Figure 6.52: Weighted primary vertex charge with $\kappa = 0.6$. a) For all selected events in data and simulation, and b) for $B_s \to \ell$ simulated events.

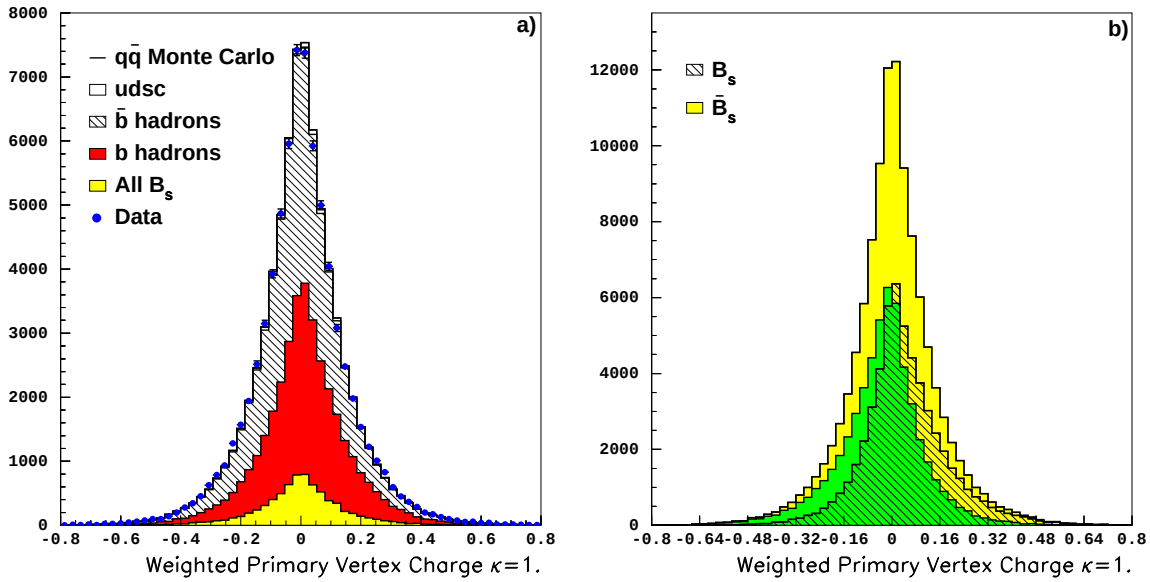

Figure 6.53: Weighted primary vertex charge with $\kappa = 1$. a) For all selected events in data and simulation, and b) for $B_s \to \ell$ simulated events.

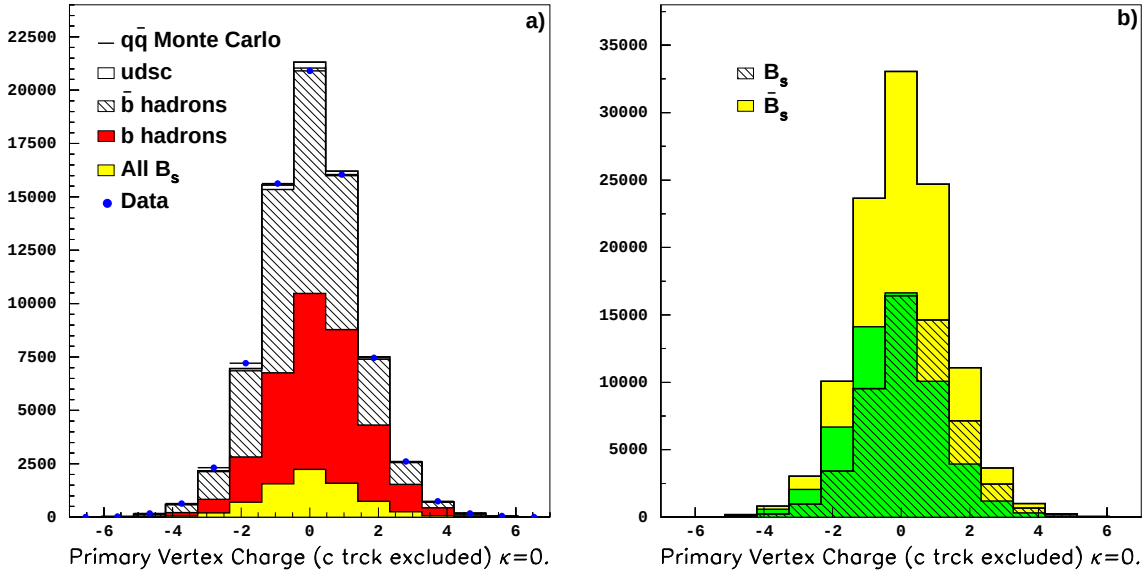

Figure 6.54: Primary vertex charge, c tracks excluded, with $\kappa = 0$. a) For all selected events in data and simulation, and b) for $B_s \to \ell$ simulated events.

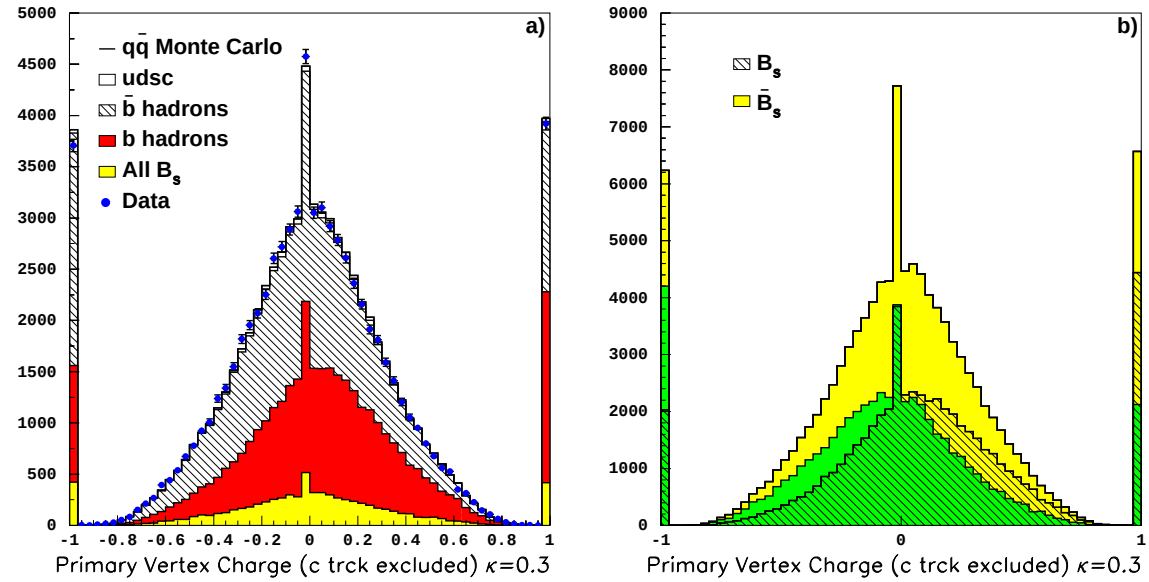

Figure 6.55: Primary vertex charge, c tracks excluded, with $\kappa = 0.3$. a) For all selected events in data and simulation, and b) for $B_s \to \ell$ simulated events.

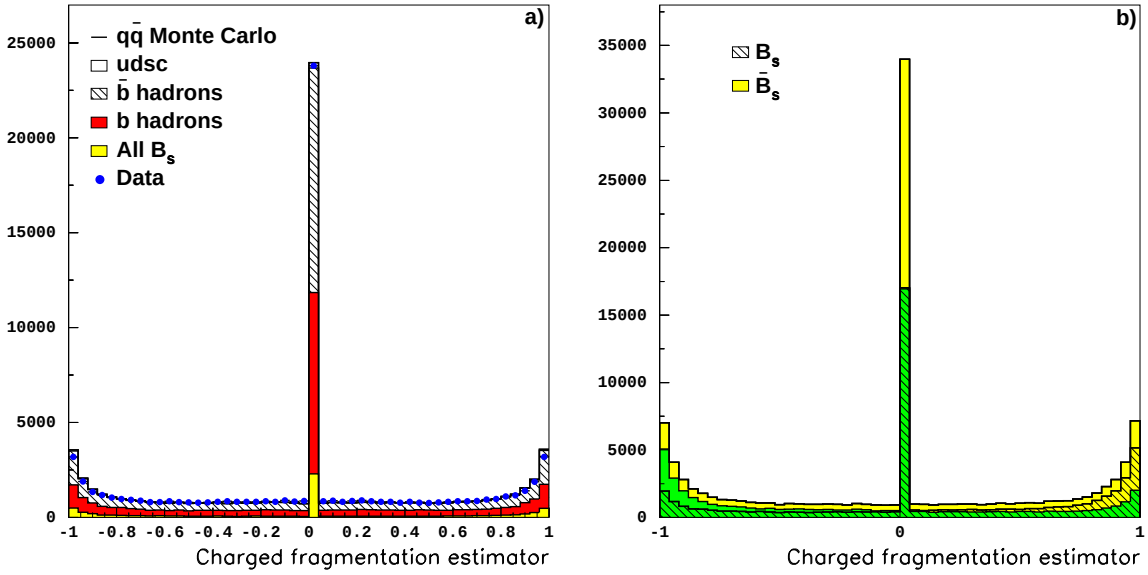

Figure 6.56: Charged fragmentation kaon estimator. a) For all selected events in data and simulation, and b) for $B_s \to \ell$ simulated events.

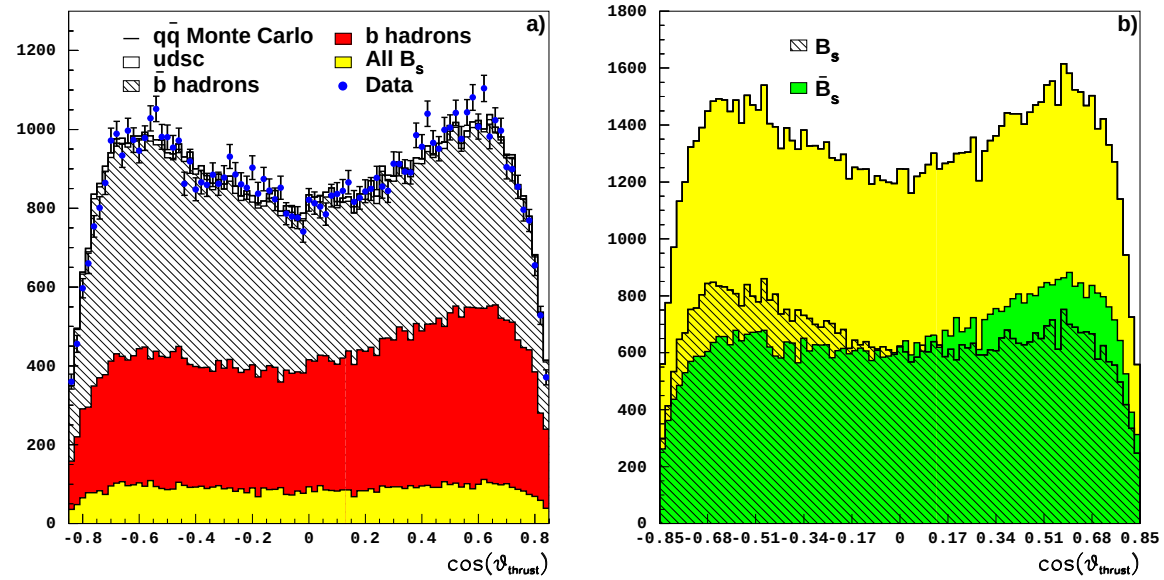

Figure 6.57: Signed thrust polar angle. a) For all selected events in data and simulation, and b) for $B_s \to \ell$ simulated events.

6.10.3 Flavour tag performance

The variables described in the previous Section are combined together with the opposite side flavour tag variable (Section 6.10.1) to obtain the combined initial state tag estimator. The combination is done with a neural network trained to distinguish $B_s \to \ell$ from $\overline{B}_s \to \ell$. The same side discriminant variables are sensitive to the true b-hadron species of the B_s decay candidate. The charged fragmentation kaon is only expected to be found in the case of a $B_s/\overline{B}_s$ decay. In the case of $B^{+/-}$ decays, the primary vertex charge is expected to have a correlation with the production flavour opposite to that found for $B_d/\overline{B}_d$ or $B_s/\overline{B}_s$.

The distribution of the combined initial state tag variable, N_{is}, is shown in Fig. 6.58a for the selected sample, and in Fig. 6.58b for $B_s \to \ell$ and $\overline{B}_s \to \ell$ simulated events.

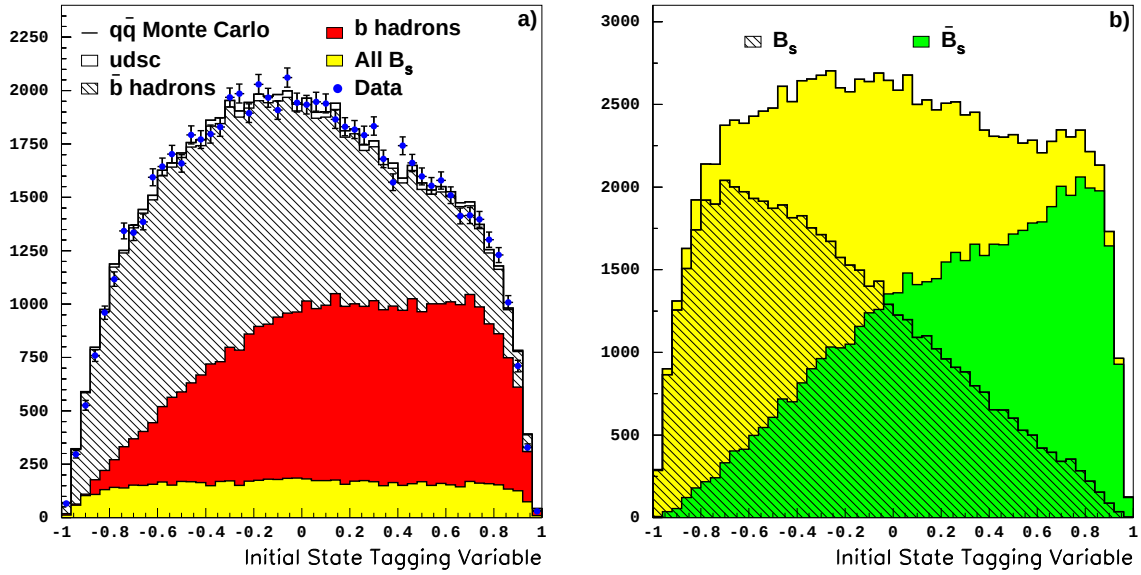

Figure 6.58: Initial state tag combined variable. a) For all selected events in data and simulation, and b) for $B_s \to \ell$ simulated events.

Events with $N_{is} < 0$ are considered as originating from a $\bar{b}$-quark. This initial state flavour is compared to the electric charge of the lepton, if $N_{is} < 0$ and the lepton charge is positive (negative), or if $N_{is} > 0$ and the lepton charge is negative (positive), the event is labeled as "unmixed" ("mixed"). This tag is used in Chapter 8 to define the probability density function to be used for each event.

The initial state tag variable, N_{is}, is translated to an event-by-event mistag probability to be used in the oscillation fit (Section 8.1.1). For $B_s \to \ell$ signal events, N_{is} is calibrated as shown in Fig. 6.59. Therefore, no particular parametrization is needed.

The effective mistag probability is defined as

$$\eta_{\text{eff}} = \frac{1}{2}\left[1 - \sqrt{\frac{\sum_i (1-\eta_i)^2 N_i^T}{\sum_i N_i^T}}\right] . \tag{6.16}$$

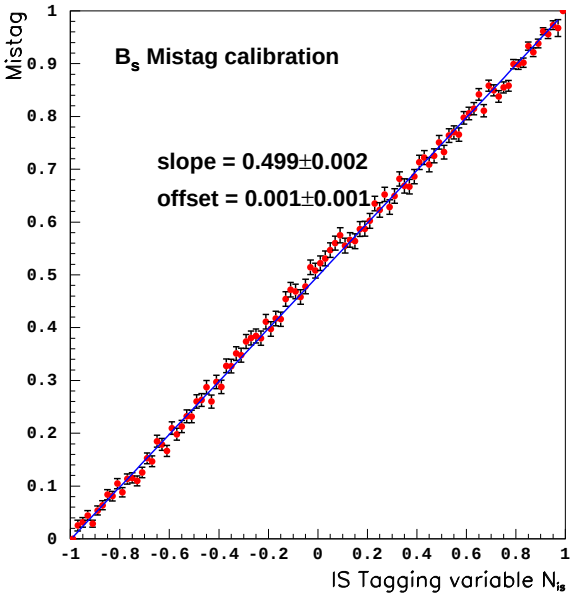

Figure 6.59: Calibration of the Initial State tag variable for $B_s \to \ell$ simulated events. The slope of the straight line fit and the offset at $N_{is} = -1$ are given.

The distribution of the discriminant variable N_{is} is divided in bins, η_i is the fraction of wrongly tagged events in each bin, and N_i^T is the total number of events in each bin. The effective mistag is used to measure the effective statistical significance which results from the tagging variable. On $B_s \to \ell$ events it is evaluated to be $\eta_{eff} = 24\%$ (while the average mistag probability is $\eta_{avg} = 28\%$).

The mistag probability needs to be parametrized as a function of the tagging variable for the other b-hadron species. The global (all vertex classes together) calibration curves for B_d, B^+, and b-baryons are shown in Fig. 6.60.

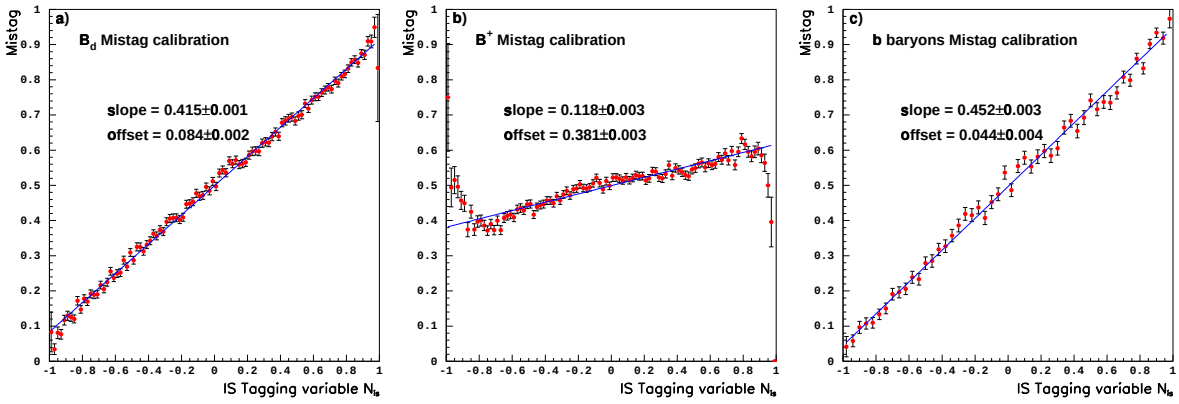

Figure 6.60: Calibration of the N_{is} variable for: a) B_d, b) B^+, and c) b-baryons. The slope of the straight line fit and the offset at $N_{is} = -1$ are given.

None of the curves in Fig. 6.60 is a perfect straight line with slope 0.5 and zero offset at $N_{\rm is} = -1$, as in the case of $B_s \to \ell$. The worst performance is observed for B^+. It is due to the opposite correlation between the primary vertex charge and the b-hadron flavour of B^+ with respect to B_s. The fact that the initial state tagging performance for the other b-hadrons is not optimal is not a problem for the B_s oscillation analysis. However the parametrization of the performance has to be done carefully not to affect the analysis result, a detailed parametrization is performed for each b-hadron species. In particular, it has been seen that, in the case of B_d mesons, the performance of the tagging depends on the measured proper time of the meson. The slope of the calibration curve is below 0.4 at low proper time ($t < 0.6\,\text{ps}$) and above 0.45 for high proper time ($t > 3\,\text{ps}$). This effect is taken into account in the event characterization used for the oscillation fit.